(4)

CONTRACT TECHNICAL REPORT

"On the Buckling/Kinking Compressive Failure of Fibrous Composites"

By

I. Chung and Y. Jack Weitsman

Prepared for: Office of Naval Research
Arlington, Virginia

Mechanics Division
Engineering Science Directorate
Contract N00014-90-J-1556

Report ESM94-2.0-CM
March 1994

Engineering Science and Mechanics
THE UNIVERSITY OF TENNESSEE
Knoxville, TN 37996-2030

UT

Unclassified

SECURITY CLASSIFICATION OF THIS PAGE

REPORT DOCUMENTATION PAGE

1a. REPORT SECURITY CLASSIFICATION Unclassified	1b. RESTRICTIVE MARKINGS
2a. SECURITY CLASSIFICATION AUTHORITY	3. DISTRIBUTION / AVAILABILITY OF REPORT Unlimited
2b. DECLASSIFICATION / DOWNGRADING SCHEDULE	
4. PERFORMING ORGANIZATION REPORT NUMBER(S)	5. MONITORING ORGANIZATION REPORT NUMBER(S)
6a. NAME OF PERFORMING ORGANIZATION Eng. Science & Mechanics University of Tennessee 6b. OFFICE SYMBOL (If applicable)	7a. NAME OF MONITORING ORGANIZATION Office of Naval Research
6c. ADDRESS (City, State, and ZIP Code) 307 Perkins Hall Knoxville, TN 37996-2030	7b. ADDRESS (City, State, and ZIP Code) Office of Naval Research , Code 432 800 N. Quincy Ave., Ballston Tower #1 Arlington, VA 22217
8a. NAME OF FUNDING / SPONSORING ORGANIZATION Office of Naval Research 8b. OFFICE SYMBOL (If applicable)	9. PROCUREMENT INSTRUMENT IDENTIFICATION NUMBER N00014-90-J-1556 (ONR Contract #)
8c. ADDRESS (City, State, and ZIP Code) Arlington, VA 22217	10. SOURCE OF FUNDING NUMBERS PROGRAM ELEMENT NO. / PROJECT NO. / TASK NO. / WORK UNIT ACCESSION NO

11. TITLE (Include Security Classification)
On the Buckling/Kinking Compressive Failure of Fibrous Composites

12. PERSONAL AUTHOR(S) I. Chung and Y. Jack Weitsman

13a. TYPE OF REPORT	13b. TIME COVERED	14. DATE OF REPORT (Year, Month, Day)	15. PAGE COUNT
Technical	FROM 10/1/92 TO 1/31/94	94-03-29	31

16. SUPPLEMENTARY NOTATION

17. COSATI CODES			18. SUBJECT TERMS (Continue on reverse if necessary and identify by block number)
FIELD	GROUP	SUB-GROUP	

19. ABSTRACT (Continue on reverse if necessary and identify by block number)

In this article it is demonstrated that the compressive response of uni-directionally reinforced composites may initiate in a micro-buckling mode and subsequently switch to a micro-kinked configuration. The foregoing possibility derives from a mechanics model which considers initial fibers misalignments, non-linear shear response of the matrix, shear deformable fibers and stochastic fiber spacings. The latter non-uniformity in fiber spacings plays a major role in the generation of fiber kinks.

Various features of the compressive deformation and failure process are exhibited by computational examples.

20. DISTRIBUTION / AVAILABILITY OF ABSTRACT ☐ UNCLASSIFIED/UNLIMITED ☐ SAME AS RPT. ☐ DTIC USERS	21. ABSTRACT SECURITY CLASSIFICATION Unclassified
22a. NAME OF RESPONSIBLE INDIVIDUAL Dr. Yapa Rajapakse	22b. TELEPHONE (Include Area Code) 703/696-4403 22c. OFFICE SYMBOL

DD FORM 1473, 84 MAR 83 APR edition may be used until exhausted. All other editions are obsolete.

SECURITY CLASSIFICATION OF THIS PAGE
Unclassified

On the Buckling/Kinking Compressive Failure of Fibrous Composites§

by

I. Chung and Y. Weitsman*
Department of Engineering Science and Mechanics
The University of Tenneseee

Abstract

In this article it is demonstrated that the compressive response of unidirectionally reinforced composites may initiate in a micro-buckling mode and subsequently switch to a micro-kinked configuration. The foregoing possibility derives from a mechanics model which considers initial fibers misalignments, non-linear shear response of the matrix, shear deformable fibers and stochastic fiber spacings. The latter non-uniformity in fiber spacings plays a major role in the generation of fiber kinks.

Various features of the compressive deformation and failure process are exhibited by computational examples.

---

§ Work supported under Contract N00014-90-J-1556 from the Office of Naval Research (ONR)

* Also at the Engineering Technology Division, Oak Ridge National Laboratory, USA

Introduction

The compressive response of composites has been studied extensively during the past three decades by many researchers. Many of the above studies are noted in comprehensive listings and review articles by Shuart (1985), Camponeschi (1991), Guynn et al. (1992) and Piggott (1993), and will not be detailed here. Suffices to say that experimental data on compressive response exhibit substantial scatter, which is partly attributable to variability of the loading mechanisms and partly due to its sensitivity to random material flaws and misalignments. On the other hand, many analytical and computational models predicted compressive strengths in excess of experimental values. This shortcoming led to an ongoing effort to construct more complicated models, which incorporate additional material and structural parameters, to achieve closer correlation between predictions and data.

An intriguing aspect of the compressive response of fibrous composites is their failure by kinking. In most circumstances post-failure inspections reveal the presence of titled bands of broken fibers, separated along oblique straight lines from the remainder of the test sample. Since the formation of these so-called kink bands does not appear accord with a buckling mode of failure, most existing models address the compressive failure of composites either as a buckling or as a kinking phenomenon, to the exclusion of the other. These models can be grouped as follows:

(1) Models which consider buckling.

These include the work of Rosen (1965), which seems to be the first article on compressive failure of composites. Considering "shear-mode buckling" that model predicted a failure stress $\sigma_{CR} = G_m/(1-\phi_f)$, where G_m is the shear modulus of the matrix and ϕ_f the fiber volume fraction. That prediction is inadequate for two reasons: (a) it gives σ_{CR} which is several times higher than experimental values, (b) the relation $\sigma_{CR} \sim 1/(1-\phi_f)$ contradicts experimental observations which show that σ_{CR} grows linearly with ϕ_f (at least up to $\phi_f \approx 0.55$) (e.g. Piggott and Harris (1980), Morley (1987)).

Several modifications to Rosen's model were introduced subsequently. Primarily, these modifications considered non-linear shear response of the matrix and initial fiber waviness (e.g. Wang (1978), Lin and Zhang (1992), Guynn et al. (1992), Highsmith et al. (1992) and others listed in the aforementioned review articles). Additional modifications included the incorporation of fibers' shear-deformation, such as by Davis (1975), or the accounting for large deformations of the fibers by Yin (1992). Though the latter model stems from a buckling formulation, it is worth noting that it

proposes a criterion for kink formation, which occurs when fibers' curvature attains a critical value.

(2) Models which consider the a-priori existence of kinks.

These include works by Evans and Adler (1978), Hahn and Williams (1986), and Budiansky and Fleck (1992).

In all the above works the fiber reinforced composites were viewed as lamellar regions which consist of fiber and matrix layers as shown in Figure 1. It should be noted that several investigators (Sadowsky et al. (1967), Herrmann et al. (1967), Lanir and Fung (1972) and Greszczuk (1975)) considered fibers of cylindrical geometry. All the latter works assumed linear elastic behavior of fiber and matrix materials.

The validity of representing fiber-reinforced materials as lamellar regions was questioned recently by Weitsman and Chung (1994), where severe disparities were shown to exist between strain fields in lamellar and arrayed fibrous geometries subjected to buckling-mode deformations. This issue is the subject of an ongoing investigation.

The main purpose of the present article is to present a model for the compressive response of fiber reinforced composites which suggests a transitional mechanism from a micro-buckling form of deformation to a micro-kinking mode of failure. The model employs the lamellar geometry of Figure 1 and incorpoates non-linear shear response of the matrix and linearly elastic, shear-deformable fibers. In addition, the model considers two kinds of geometrical imperfections, initial fiber misalignments and non-uniform fiber spacing. The latter consideration is the novel aspect of this work. In closely spaced fibrous domains the narrow matrix regions sustain increased levels of shear strains which approach yield or failure limits. The resulting softening in the support provided by the matrix to the fibers is shown to cause localized fiber failures, accompained by overburdening the more widely spaced fibers. Though compressive failure still occurs by buckling, the immediate post-buckled configuration is shown to consist of kinked fibers. The sudden transition from buckling to kinking is due to the abrupt variation in the deformed configuration which follows the buckling instability. This comprehensive accounting for the seemingly disparate phenomena of buckling and kinking is the main asset of the present model.

Non-uniform fiber spacings were considered by Chung and Weitsman in a previous work (1993). However, in that work the fibers were modelled as Bernoulli-Euler beams and, in the absence of shear deformations, could not develop kinks. It is interesting to note that under the constraints inherent in the Bernoulli-Euler beam theory the absence of kinks was compensated by the presence of highly concentrated shear forces in the post-buckling range of

response. An abbreviated version of the current article with computational results based upon material data reported by Guynn et al. (1992) is due to appear in the Proceedings of the Twelfth U. S. National Congress of Applied Mechanics (I. Chung and Y. J. Weitsman, 1994).

Basic Equations

Let a uni-directionally reinforced fibrous composite be represented by a layered medium which consists of fiber and matrix layers of thicknesses 2h and 2(c-h), respectively as shown in Figure 1. Let $\phi_f = h/c$ and $\phi_m = (c-h)/c$ denote volume fractions where here, and in the remainder of this article, subscripts f and m refer to the fiber and matrix, respectively. Let x and y denote coordinates parallel and normal to the layers, with corresponding displacements u and v.

Consider an initial waviness v_0 in the fiber layer, given by

$$v_0 = \delta_0 \cos(\pi x/L) \tag{1}$$

and let the fibers deflect in a shear mode of buckling as shown in Figure 2. (Rosen (1965), Garg et al. (1973)).

The length L prescribes the micro-buckling length associated with compressive loading N parallel to the fibers. We assume that the matrix layer responds in shear only, sharing a common displacement v with the fiber, while u_m varies linearly in x across the layer's thickness. In addition, we suppose that the deformation within the fiber layer is expressed by Timoshenko's shear-deformation model, where Ψ denotes the independent rotation of the planar cross-section.

Accounting for bending effects, the total displacement of a fiber region U_f is given by (Washizu (1975))

$$U_f = u_f + \frac{1}{2}\int_0^x \left[\left(v' + v_0'\right)^2 - \left(v_0'\right)^2 \right] dx - y\psi \tag{2}$$

with the corresponding strains

$$\varepsilon_x^f = u_f' + \frac{1}{2}\left[\left(v' + v_0'\right)^2 - \left(v_0'\right)^2 \right] - y\psi' \tag{3a}$$

$$\gamma^f_{xy} = v' - \psi \tag{3b}$$

while

$$\gamma^m_{xy} = \frac{\partial v}{\partial x} + \frac{\partial u_m}{\partial y} = v' + \frac{1}{2(c-h)}\left[U_f(x, 2c-h) - U_f(x, h)\right]$$

$$= v' - \frac{\phi_f}{\phi_m}\frac{\partial U_f}{\partial y} = v' + \frac{\phi_f}{\phi_m}\psi \tag{4}$$

In equations (2) - (4), and in the sequel, primes denote derivatives with respect to x.

Consider linear elastic response for the fibers

$$\sigma^f_x = E_f \varepsilon^f_x, \quad \tau^f_{xy} = G_f \gamma^f_{xy} \tag{5}$$

and a non-linear shear response for the matrix, scaled by the initial shear modulus G^e_m

$$\tau^m_{xy} = G^e_m \, F(\gamma^m_{xy}) \tag{6}$$

The total relative deflection between x = 0 and x = L/2 (say) is given by

$$\Delta = u_f(L/2) + \frac{1}{2}\int_0^{L/2} \left[\left(v' + v_0'\right)^2 - \left(v_0'\right)^2\right] dx \tag{7}$$

Random Fiber Spacing

As noted in the Introduction, random fiber spacing accounts for an essentially novel feature in the present model. Following basic statistical notions concerning the subdivision of a linear segment into M sub-segments of random lengths (Dixon and Massey (1969)), we assume that the cell sizes 2c are distributed according to a Poisson's point process, with a cumulative distribution function

$$P(C > c) = \exp(-c/\bar{c}) \tag{8}$$

In equation (8) $2\bar{c}$ is the nominal average of the cell sizes. Since fiber regions cannot overlap, namely $c > h$ ("Gibbs hard core process"), equation (8) is modified to read

$$P(C > c) = \exp\left(-\frac{c-h}{\bar{c}-h}\right) \tag{9}$$

The corresponding probability distribution is

$$p(c) = -\frac{1}{\bar{c}-h}\exp\left(-\frac{c-h}{\bar{c}-h}\right) \tag{10}$$

In the sequel we shall need to refer to the probability distribution of the fiber volume fractions $p(\phi_f)$, where $\phi_f = \frac{h}{c}$. Employing well established rules of statistical analysis we obtain

$$p(\phi_f) = \frac{\bar{\phi}_f}{\phi_m}\frac{1}{\phi_f^2}\exp\left(-\frac{\bar{\phi}_f}{\phi_m}\frac{\phi_m}{\phi_f}\right) \tag{11}$$

For computational purposes the distribution function $p(\phi_f)$ will be discretized and expressed by a finite number of Dirac delta functions.

Field Equations for Randomly Spaced Layers In Compression

In view of equation (4), and subsequently equation (6), it follows that both γ_{xy}^m and τ_{xy}^m are functions of the ranodm variable ϕ_f and thereby random as well. However, to ascertain common displacement Δ for all layers we assume identical displacements u and v for all layers inspite of the randomness in their widths 2c. We posit that the effects of random spacing are taken up by distinct values of the rotation Ψ, which vary from layer to layer. Consequently, a descretized version of $p(\phi_f)$ which corresponds to M values of $(\phi_f)_i$ $(i = 1, \ldots M)$ will necessitate the consideration of M values of Ψ_i $(i = 1, \ldots M)$.

The above assumption involves an approximation whose validity can be estimated. It will be shown below that a solution for u, v, $\Psi_1, \ldots \Psi_M$ which is based upon energy considerations for the entire composite fails to satisfy

equilibrium conditions for any of the M individual layers. The magnitudes of the unequilibrated transverse forces (distributed transverse loads $q_i(x)$, i = 1, . . . M) provide the required estimate of error. It turns out that the above magnitudes never exceed 1% of all calculated stress values, attesting to the suitability of the approximation.

Application of the principle of virtual work to the entire composite (Washizu (1975)), upon accounting for the randomness of the cell sizes c, yields,

$$\int_h^\infty p(c) \left\{ \int_{V_f} \left(\sigma_x^f \, \delta\varepsilon_x^f + \tau_{xy}^f \, \delta\gamma_{xy}^f \right) dV_f + \int_{V_m} \tau_{xy}^m \, \delta\gamma_{xy}^m \, dV_m \right\}_{(c)} dc + N\delta\Delta = 0 \qquad (12)$$

In view of expressions (3) through (6), which contain the random variables ϕ_f and ϕ_m, and since by hypothesis Ψ depends on c, it follows that the expression within the curly brackets on the left side of equation (12) is a function of the random variable c.

Consider a discrete probability distribution, represented by W_i, commesurate with equations (10) and (11), which corresponds to M cells of widths $2c_i$ (i= 1, . . . M). In this case the integral in equation (12) is replaced by a sum and we obtain

$$2 \sum_{i=1}^{M} W_i \int_0^{L/2} \left\{ \int_0^h \left(\sigma_x^f \, \delta\varepsilon_x^f + \tau_{xy}^f \, \delta\gamma_{xy}^f \right) dy + \int_h^{c_i} \tau_{xy}^m \, \delta\gamma_{xy}^m \, dy \right\} dx + N\delta\Delta = 0 \qquad (13)$$

Note that $\delta\varepsilon_x^f$, $\delta\gamma_{xy}^f$ and $\delta\gamma_{xy}^m$ contain M + 2 independent variations, namely δu, $\delta v'$ and $\delta\psi_i$ (i = 1, . . . M).

Substitution of equations (2) - (7) into expression (13), integrating by parts and collecting terms which multiply δu, $\delta v'$ and $\delta\psi_i$ (i = 1, . . . M), we obtain the following (M + 1) field equations for v and Ψ_i (i = 1, . . . M)

$$-N\left(v' + v_0'\right) + 2h \sum_{i=1}^{M} \left\{ G_f\left(v' - \psi_i\right) + \left(\phi_m/\phi_f\right)_i \, G_m^e F\left[v' + \left(\phi_f/\phi_m\right)_i \psi_i \right] \right\} = 0 \qquad (14)$$

$$- E_f I_f \psi_i'' - 2hG_f\left(v' - \psi_i\right) + 2hG_m^e F\left[v' + \left(\phi_f/\phi_m\right)_i \psi_i\right] = 0 \quad (i = 1, \ldots M) \tag{15}$$

with the boundary conditions

$$\psi_i'(L/2) = 0, \quad \psi_i(0) = 0 \quad (i = 1, \ldots M), \quad \text{and } v'(0) = 0. \tag{16}$$

Note that the coupled system of equations (14) and (15) is non-linear due to the presence of the function F, which is non-linear in its argument.

In equations (15) $I_f = h^3/12$. Note that the variation δu yields the trivial result N = constant = $N_{applied}$, and requires no further consideration.

Unlike equations (15), which apply to the M individual cells, equation (14) expresses the lateral equilibrium of the entire composite. To ascertain lateral equilibrium of each cell it is necessary to impose distributed transverse loads $q_i(x)$ (i=1, . . . M) and consider their virtual work $\int_0^{L/2} q_i \delta v dx$.

Reemployment of the principle of virtual work for each individual cell, collecting terms that multiply δv and utilizing the solution for v and ψ_i which corresponds to the system of equations (14) - (16), we get

$$q_i = N\left(v'' + v_0''\right) - 2h \sum_{i=1}^{M} \left\{G_f\left(v'' - \psi_i'\right) + \left(\phi_m/\phi_f\right)_i G_m^e F'\left[v' + \left(\phi_f/\phi_m\right)_i \psi_i\right]\right\} \tag{17}$$

The relative magnitudes of q_i/τ_{xy}^m serve as measures for the validity of the approximation inherent in assuming common u and v in all layers. It will be shown in the next section that for polymeric composites all the above ratios appear to be less than 10^{-2}.

A non-dimensional version of equations (14) and (15) is obtained upon introducing X = x/L, V = v/L and the non-dimensional factors $\alpha_f^2 = \frac{2G_f hL^2}{E_f I_f}$, $\alpha_m^2 = \frac{2G_m^e hL^2}{E_f I_f}$, $\lambda^2 = \frac{NL^2}{E_f I_f}$.

Then upon denoting Y = dV/dX, equations (14) and (15) read

$$-\lambda^2(Y+Y_0)+\alpha_f^2 Y+\sum_{i=1}^{M} W_i\left\{-\alpha_f^2\psi_i+\left(\phi_m/\phi_f\right)_i \alpha_m^2 F\left[Y+\left(\phi_f/\phi_m\right)_i\psi_i\right]\right\}=0 \qquad (18)$$

and

$$\psi_i'' + \alpha_f^2\left(Y-\psi_i\right)-\alpha_m^2 F\left[Y+\left(\phi_f/\phi_m\right)_i\psi_i\right]=0 \quad (i=1,\ldots M) \qquad (19)$$

with the boundary conditions

$$\psi_i'(1/2)=0,\ \psi_i(0)=0,\ (i=1,\ldots M) \text{ and } Y(0)=0. \qquad (20)$$

Results

The solution to equations (18) - (20) was obtained numerically and pertains to graphite/PEEK (APC-2) composites. The interval $0 < X < 1/2$ was subdivided into K equal sub-intervals and derivatives were expressed by means of central finite differences. The discretized system of equations was solved iteratively to obtain values of V and Ψ_i for increasing load N in the pre-buckling range. In accordance with observations by Johnson et al. (1991) the matrix material was assumed fail in those regions where $\gamma_{xy}^m \geq 0.05$. The response in the post-buckling range was evaluated by prescribing the location X^* where $\gamma_{xy}^m = 0.05$ in the most recently failed cells and evaluating the corresponding deflected shape V(X) and applied load N.

Complete details are given in the Appendix.

The computations employed values of $E_f = 214$ GPa and $G_f = 13.8$ GPa, which reflect the significant transverse isotropy of the AS4 fibers (Aboudi (1991)). The in-situ shear stress-strain response of the PEEK resin was based upon the reduction of data collected by Kyriakides and Liechti (1993). The in-situ data are shown in Figure 3, where they are contrasted with data for unreinforced PEEK.

The in-situ shear data were expressed by the relation $\gamma=\frac{\tau}{A}+\left(\frac{\tau}{B}\right)^q$ where A = 3096 MPa, B = 169.93 MPa, q = 0.23781 and τ in MPa. As noted earlier, shear failure was assumed to occur at a strain of $\gamma_u = 0.05$. In addition, we took

$L = 400d$ and $\delta_0 = 4d$, as suggested by Kyriakides and Liechti (1993), with a fiber diameter $d = 7.6\ \mu m$.

The computational scheme considered four random cell sizes, namely four discrete random values of ϕ_f which accord with the distribution function of equation (11). These are shown in Figure 4.

Computaitonal results are shown in Figures 5 - 12.

Figure 5 exhibits the variation of the applies stress σ vs. the non-dimensionalized maximal lateral deflection $v(0)/h$. The short plateau-like region at $1.5 < v(0)/h < 1.8$ is due to matrix failure which initiates and spreads within the cell with highest fiber volume fraction ($\phi_f = 0.975$). Failure by buckling occurs at $\sigma = 1220$ MPa (point A). In a displacemnt controlled experiment a further increase in Δ will be accompanied by a drop in σ and a corresponding reduction in $v(0)/h$. The post buckling response is represented by the segment AB in Figure 5.

Results for the non-dimensionalized displacement V and slope Y are plotted versus the non-dimensional distance X in Figures 6 and 7 for various load levels in both pre and post buckling ranges. As may be expected, these curves are approximately proportional to cos X and sin X in the pre-buckling range, where deformed shapes are dominated by the form of the initial misalignment. Note, however, the substantial deviations in the deformed configurations within the post-buckling range, where they no longer resemble the cos X shape of the initial misalignment. The most significant departures occur near $X = 0.5$, where matrix failures initiate.

The distributions of τ_{xy}^m versus X are plotted in Figures 8(a) through 8(d). These distributions are shown within the four distinct cells and for various levels of applied stress. Figure 8(a) corresponds to a pre-buckled stress level $\sigma = 654$ MPa, Figure 8(b) corresponds to the buckling stress $\sigma = 1220$ MPa (point A in Figure 5) when the matrix within the cell with $\phi_f = 0.975$ failed over the range $0.16 < X < 0.5$.

Figures 8(c) and 8(d) correspond to post-buckling loads of $\sigma = 730$ MPa and $\sigma = 722$ MPa, respectively. The latter stress corresponds to point B in Figure 5, which lies directly below point A in that figure. Note the spreading of the failure region in the cell with $\phi_f = 0.8$ between the post-buckling stages depicted in Figures 8(c) and 8(d). Namely, matrix failure which was confined to $0.49 < X < 0.5$ at $\sigma = 730$ MPa expanded over $0.45 < X < 0.5$ as the post

buckling load level proceeded to drop to σ = 7.22 MPa. There were also increases in τ^m_{xy} within the unfailed cells with ϕ_f = 0.45 and ϕ_f = 0.175.

The central theme of the present article is demonstrated in Figures 9(a) through 9(d). Those figures exhibit the fiber shear strains γ^f_{xy} versus the non-dimensional distance X for the same circumstances as in Figures 8(a) - 8(d). The essential feature of those figures develops within the post-buckling range, where discontinuities in γ^f_{xy} are noted to occur simultaneously within all cells. These discontinuities are located at X = 0.49 in Figure 9(c) and at X = 0.45 in Figure 9(d). No such discontinuities exist in the pre-buckling stage or at buckling.

We suggest that the foregoing discontinuities in γ^f_{xy} portend the onset of fiber kinking.

Figure 10(a) exhibits the computed values of the lateral loads $q_j(X)$ versus X within all four cells at buckling, namely at σ = 1220 MPa. These loads, which were evaluated through equation (17), are much smaller than τ_u = 70 MPa, attesting to the validity of the premises of the present model. For purposes of comparison, the same lateral loads are plotted versus X in Figure 10(b) when the fibers are modelled as Bernoulli-Euler beams, employing a previous analysis by Chung and Weitsman (1993).

Additional effects of random fiber spacings are exhibited in Figures 11 and 12. Figures 11(a) and 11(b) concern the evolution of fiber curvatures with load within the pre-buckling range and demonstrate the contrast between uniformly spaced and randomly spaced circumstances. It may be noted that the randomly spaced case gives rise to highly concentrated curvatures, with magnitudes which exceed by three or four folds the levels which correspond to the uniformly spaced case. If one accepts the premise of Yin (1992) that kinks occur when fiber's curvature exceeds a certain threshold level, then the current analysis indicates the existence of an enhanced likelihood of kinking due to non-uniform fiber spacing. Such kinking may preceed failure by buckling.

Finally, the effect of random fiber spacing on compressive strength is shown in Figure 12, where buckling failure loads are plotted versus the fiber volume fraction ϕ_f. The results for the random case were computed for average values $\bar{\phi}_f$ (with the distribution shown in Figure 4) that are identical with the constant ϕ_f for the uniformly spaced case. Note that random fiber

spacings result in lower strengths with $\bar{\phi}_f$, which accords with experimental observations by Piggott and Harris (1980).

Conclusions

A mechanics model was presented for the compressive response and failure of uni-directionally reinforced polymeric composites loaded parallel to the fiber direction. The analysis accounted for the non-linear shear response of the resin, including its ultimate shear strain, and for shear deformable fibers. The model incorporated two kinds of geometric imperfections, namely, initial fiber waviness and random fiber spacings. Excepting the works by Chung and Weitsman (1993, 1994), the latter kind of imperfection has not been considered elsewhere.

Computational results were evaluated within both pre and post-buckling ranges of compressive response. The paramount result of this work is an indication that a band of discontinuity in the fibers' shear strains can occur immediately beyond failure by buckling. Such a discontinuity may portend the formation of kink bands which are observed in many failed specimens.

In addition, it was shown that an accounting for random fiber spacings reduces the predicted values of compressive strength and results in a correlaiton between the above strength and fiber volume fractions which concurs with experimentally observed trends.

Acknowledgement

This work was performed under Contract N00014-90-J-1556 from the Office of Naval Research to one of the authors (YW). The authors wish to thank the program manager, Dr. Y. Rajapakse of the Mechanics Division, Engineering Sciences Directorate, for his encouragement and support.

References

Aboudi, J. (1991). Mechanics of Composite Materials. Elseveier (p. 55).

Budiansky, B. and Fleck, N. A. (1992). Compressive Failure of Fibre Composites. *Journal of Mechanics and Physics of Solids*, 41, 193-211.

Camponeschi, E. T., Jr. (1991). Compression of composite Materials: A Review. *Composite Materials: Fatigue and Fracture, ASTM STP 1110,* 550-578.

Chung, I. and Weitsman, Y. J. (1993). A Mechanics Model for the Compressive Response of Fiber Reinforced Composites. Report ESM93-2.0-CM, Department of Engineering Science and Mechanics, The University of Tennessee (To appear in the International Journal of Solids and Structures).

Chung, I. and Weitsman, Y.J. (1993). A Model for the Micro-Buckling/Micro-Kinking Compressive Response of Fiber-Reinforced Composites (To appear in Proceedings of the 12th U. S. National Conference of Applied Mechanics, Seattle, WA, 1994).

Davis, Jr., J. G. (1975). Compressive Strength of Fiber-Reinforced Composite Materials. *Composite Reliability, ASTM STP 580,* 364-377.

Davy, P. J. and Guild, F. J. (1988). The Distribution of Interparticle Distance and Its Application in Finite Element Modeling of Composite Materials. *Proceedings of Royal Society,* A418, 95-112.

Dixon, W. J. and Massey, F. J. (1969). Introduction to Statistical Analysis. McGraw Hill-Kogakusha.

Evans, A. G. and Adler, W. F. (1978). Kinking as a Mode of Structural Degradation in Cabon fiber Composites. *Acta Metallurgica,* 26, 725-738.

Garg, S. K., Svalbonas, V., and Gurtman, G. A. (1973). Analysis of Structural Composite Materials, M. Dekker Inc., New York.

Greszczuk, L. B. (1975). Microbuckling Failure of Circular Fiber-Reinforced Composites. *AIAA Journal,* 13, 1311-1318.

Guynn, E. G., Ochoa, O. O., and Bradley, W. L. (1992). A Parametric Study of Variables That Affect Fiber Microbuckling Initiation in Composite Laminates: Part 1 Analyses. *Journal of Composite Materials,* 26, 1594-1616.

Hahn, H. T. and Williams, J. G. (1986). Compression Failure Mechanisms in Unidirectional Composites. *Composite Materials: Testing and Design, ASTM STP 893,* 115-139.

Hermann, L. R., Mason, W. E., and Chan, S. T. K. (1967). Response of Reinforcing Wires to Compressive States of Stress. *Journal of Composite Materials,* 1, 212-226.

Highsmith, A. L., Davis, J. J., and Helms, K. L. E. (1992). The Influence of Fiber Waviness on the Compressive Behavior of Unidirectional Continuous Fiber Composites. *Composite Materials: Testing and Design, ASTM STP 1120*, 20-36.

Johnston, N. J., Towell, T. W., and Hergenrother, P. M. (1991). Physical and Mechanical Properties of High Performance Thermoplastic Polymers and Their Composites. *Thermoplastic Composite Materials* edited by Carlsson, L. A., Elsevier Science Publishers, 27-71.

Kyriakides, S. and Liechti, K. M. (1993). Private communication.

Lanir, Y. and Fung, Y. C. B. (1972). Fiber Composite Columns under Compression. *Journal of Composite Materials*, 6, 387-401.

Lin, K. Y. and Zhang, X. J. (1992). Effect of Fiber Waviness on the Compressive Strength of Laminated Composites. *Proceedings of the 2nd International Symposium on Composite Materials and Structures*, Beijing, China, 120-125.

Morley, J. G. (1987). High Performance Fiber Composites, Academic Press.

Na, T. Y. (1979). Computational Methods in Engineering Boundary Value Problems, Academic Press.

Piggott, M. R. and Harris, B. (1980). Compression Strength of Carbon, Glass and Kevlar-49 Fibre Reinforced Polyester Resins. *Journal of Materials Science*, 15, 2523-2538.

Piggott, M. R. (1993). Compressive Strength of Composites: How to Measure It and How to Improve It. Advanced Composites '93. *Proceedings of the International Conference on Advanced Composite Materials (ICACM)*, Wollongong, Australia, February 15-19, 1993. (Chandra and Dhingra, Eds.) pp. 51-59 TMS. Publication.

Rosen, B. W. (1965). Mechanics of Composite Strengthening. *Fiber Composite Materials*, American Society for Metals, 37-75.

Sadowsky, M. A., Pu, S. L. and Hussain, M. A. (1967). Buckling of Microfibers. *Journal of Applied Mechanics*, 34, 1011-1016.

Wang, A. S. D. (1978). A Nonlinear Microbuckling Model Predicting the Compressive Strength of Unidirectional Composites. *ASME Paper 78-WA/Aero-1*, 1-8.

Washizu, K. (1975). Variational Methods in Elasticity and Plasticity. Pergamon Press.

Weitsman, Y. and Chung, I. (1994). Can the Compressive Response of Fiber-Reinforced Composites be Modelled by Layered Arrays? Report ESM94-1.0-CM, Department of Engineering Science and Mechanics, The University of Tennessee.

Yin, W. L. (1992). A New Theory of Kink Band Formation. *AIAA-92-2552-CP*, 3028-3035.

Appendix

Upon denoting $\xi_i = \frac{d\psi_i}{dX}$, the non-dimensionalized governing equations (18) and (19) read

$$-\lambda^2(Y+Y_0) + \alpha_f^2 Y + \sum_{i=1}^{M} w_i\left(-\alpha_f^2 y_i + \alpha_m^2 \frac{\phi_{mi}}{\phi_{fi}} F_i\right) = 0$$

$$\frac{d\xi_i}{dX} + \alpha_f^2(Y - \psi_i) - \alpha_m^2 F_i = 0 \qquad \text{(A-1)}$$

$$\frac{d\psi_i}{dX} = \xi_i \qquad (i = 1, \ldots M)$$

The first equation applies to the entire composite, as implied by the summation over all the Voronoi cells, while the second and third apply to the M individual cells. We thus have 2M+1 equations. This system of nonlinear coupled differential equations can be converted into algebraic equations by means of finite differences.

Let N denote the number of nodes along the buckling span, resulting in N-1 intervals of length ΔX and mid-nodes. For the mid node between n and n+1 th nodes, which is indicated by n+1/2 in the following, the finite difference version of (A-1) is

$$-\lambda^2(Y_{n+1/2}+Y_{0,n+1/2}) + \alpha_f^2 Y_{n+1/2} + \sum_{i=1}^{M} w_i\left(-\alpha_f^2 \psi_{i,n+1/2} + \alpha_m^2 \frac{\phi_{mi}}{\phi_{fi}} F_{i,n+1/2}\right) = 0$$

$$\frac{\xi_{i,n+1}-\xi_{i,n}}{\Delta X} + \alpha_f^2(Y_{n+1/2} - \psi_{i,n+1/2}) - \alpha_m^2 F_{i,n+1/2} = 0 \qquad \text{(A-2)}$$

$$\frac{\psi_{i,n+1}-\psi_{i,n}}{\Delta X} = \xi_{i,n+1/2}$$

At this stage, the non-linearity due to non-linear matrix response expressed by $F(\gamma_{xy})$ is still retained within the system. This non-linearity can be eliminated by considering the incremented quantities $Y+\delta Y$, $\xi+\delta\xi$, and $\psi+\delta\psi$ which satisfy equations (A-2). Linearization is then achieved upon

expanding the non-linear terms in Taylor series, and retaining the first order terms only. Then, the first of equations (A-2) results in

$$\delta Y_{n+1/2} = \frac{1}{\sum_{i=1}^{M} w_i Q_{i,n+1/2} - \lambda^2} \left(R_{n+1/2} + \sum_{i=1}^{M} w_i P_{i,n+1/2} \delta\psi_{i,n+1/2} \right) \qquad \text{(A-3)}$$

where

$$P_{i,n+1/2} = \alpha_f^2 - \alpha_m^2 \left(\frac{dF}{d\gamma} \right)_{i,n+1/2}$$

$$Q_{i,n+1/2} = \alpha_f^2 + \alpha_m^2 \frac{\phi_{fi}}{\phi_{mi}} \left(\frac{dF}{d\gamma} \right)_{i,n+1/2}$$

$$R_{n+1/2} = \lambda^2 \left(Y_{n+1/2} + Y_{0,n+1/2} \right) - \alpha_f^2 Y_{n+1/2} + \sum_{i=1}^{M} w_i \left(\alpha_f^2 \psi_{i,n+1/2} - \alpha_m^2 \frac{\phi_{mi}}{\phi_{fi}} F_{i,n+1/2} \right)$$

As shown in equation (A-3), δY, which is common to all cells, can be represented explicitly in terms of other variables $\delta\psi_i$. This enables the substitution of δY into the remaining equations in (A-2). The substitution of (A-3) into the truncated Taylor expansions of the last two of equations (A-2) yields the following:

$$\frac{\delta\xi_{i,n+1} - \delta\xi_{i,n}}{\Delta X} + \sum_{k=1}^{M} T_{k,i,n+1/2} \left(\delta\psi_{k,n+1} + \delta\psi_{k,n} \right) - \frac{Q_{i,n+1/2}}{2} \left(\delta\psi_{i,n+1} + \delta\psi_{i,n} \right) = U_{i,n+1/2} \qquad \text{(A-4)}$$

$$- \frac{\delta\xi_{i,n+1} + \delta\xi_{i,n}}{2} + \frac{\delta\psi_{i,n+1} - \delta\psi_{i,n}}{\Delta X} = V_{i,n+1/2}$$

where

$$S_{i,n+1/2} = - \frac{\xi_{i,n+1} - \xi_{i,n}}{\Delta X} - \alpha_f^2 \left(Y_{n+1/2} - \psi_{i,n+1/2} \right) + \alpha_m^2 F_{i,n+1/2}$$

$$T_{k,i,n+1/2} = \frac{w_k P_{k,n+1/2} P_{i,n+1/2}}{2\left(\sum_{i=1}^{M} w_i Q_{i,n+1/2} - \lambda^2\right)}$$

$$U_{i,n+1/2} = S_{i,n+1/2} - \frac{P_{i,n+1/2} R_{n+1/2}}{\left(\sum_{i=1}^{M} w_i Q_{i,n+1/2} - \lambda^2\right)}$$

$$V_{i,n+1/2} = -\frac{\psi_{i,n+1} - \psi_{i,n}}{\Delta X} + \xi_{i,n+1/2}$$

It should be noted that equations (A-4) apply to each individual cell. Thus, we have M values of ξ_i and ψ_i at any mid node. Collecting $\delta\xi_i$ and $\delta\psi_i$'s and forming the vectors

$$\{\delta\xi\} = \{\delta\xi_1, \delta\xi_2, \ldots \delta\xi_M\}^T$$

$$\{\delta\psi\} = \{\delta\psi_1, \delta\psi_2, \ldots \delta\psi_M\}^T$$

equation (A-4) can be expressed in matrix notation as

$$[B_n]\left\{\begin{Bmatrix}\{\delta\xi_{n-1}\}\\ \{\delta\psi_n\}\end{Bmatrix}\right\} + [A_n]\left\{\begin{Bmatrix}\{\delta\xi_n\}\\ \{\delta\psi_{n+1}\}\end{Bmatrix}\right\} + [C_n]\left\{\begin{Bmatrix}\{\delta\xi_{n+1}\}\\ \{\delta\psi_{n+2}\}\end{Bmatrix}\right\} = \{D_n\} \qquad \text{(A-5)}$$

Here, the A_n, B_n, and C_n are 2M by 2M matrices, and D_n is a 2M by 1 vector. Their components are given by

$$B_n(i,M+i) = -\frac{1}{\Delta X}$$

$$B_n(M+i,M+k) = T_{k,i,n+1/2}$$

$$B_n(M+i,M+i) = T_{i,i,n+1/2} - \frac{Q_{i,n+1/2}}{2}$$

$$A_n(i,i) = -\frac{1}{2}$$

$$A_n(i,M+i) = \frac{1}{\Delta X}$$

$$A_n(M+i,i) = -\frac{1}{\Delta X}$$

$$A_n(M+i,M+k) = T_{k,i,n+1/2}$$

$$A_n(M+i,M+i) = T_{i,i,n+1/2} - \frac{Q_{i,n+1/2}}{2}$$

$$C_n(i,i) = -\frac{1}{2}$$

$$C_n(M+i,i) = \frac{1}{\Delta X}$$

$$D_n(i) = V_{i,n+1/2}$$

$$D_n(M+i) = U_{i,n+1/2}$$

In the above the ranges of k and i are k=1, . . . i-1, i+1, . . . M, and i=1, . . . M, respectively.

Denote $\{\{\delta\xi\}\ \{\delta\psi\}\}^T$ by $\{\Phi\}$. Then, the governing equation for the entire length of the composite is obtained by collecting equation (A-5). Therefore,

$$\begin{bmatrix} [A_1] & [C_1] & & & 0 \\ [B_2] & [A_2] & [C_2] & & \\ & & \ddots & & \\ & & [B_{N-2}] & [A_{N-2}] & [C_{N-2}] \\ 0 & & & [B_{N-1}] & [A_{N-1}] \end{bmatrix} \begin{Bmatrix} \{\Phi_1\} \\ \{\Phi_2\} \\ \vdots \\ \{\Phi_{N-2}\} \\ \{\Phi_{N-1}\} \end{Bmatrix} = \begin{Bmatrix} \{D_1\} \\ \{D_2\} \\ \vdots \\ \{D_{N-2}\} \\ \{D_{N-1}\} \end{Bmatrix} \qquad \text{(A-6)}$$

This banded algebraic equation can be readily solved by means of the LU decomposition (Na (1979)). Since the solution Φ is a vector of increments, it is accumulated at each iterative step to compute ξ and ψ. At the end of each iteration, the norm of Φ is calculated to check for convergence. When it becomes sufficiently small, the iteration is halted, and cumulative values of ξ and ψ are regarded as the convergent solution. δY is computed by using equation (A-3) and accumulated in the same manner to obtain Y. Deflection, curvature, stress components and other quantities are computed by means of a post processing subroutine.

To determine the buckling load, both low and high bounds of applied stress and number of computation intervals are inputed in the program. The highest load value which still gives a convergent solution is taken to be the buckling load.

As shown in Figure 5, an unloading process is observed in the post-buckling regime. In contrast with the presumed linear elastic behavior of fiber, it is necessary to clearly define the stiffness of the matrix during unloading. For that purpose, isotropic hardening and elastic unloading of matrix were assumed.

The post-buckling analysis employs the buckling solution as a starting stage, which establishes all the initial values of strains and displacements that correspond to the buckling load, P_{cr}. The post-buckling computation postulates a location X^* in the most recently failed cell, which extends the region of failed matrix in that cell to $X^*<X<1/2$. Consequently, that region, like previously failed matrix regions under P_{cr}, does not contribute to the shear stiffness of the composite. Subsequently, the composite is subjected to an assumed load level $P<P_{cr}$ and the numerical scheme is employed to obtain values of all corresponding stresses and strains. Note that wherever the scheme predicts unloading, it is programmed to follow a linear elastic unloading path of the matrix. The value of γ at the foregoing location X^* is then compared with γ_u. If $\gamma(X^*) > \gamma_u$ the level of the load P is reduced iteratively until the establishment of equality, $\gamma(X^*) = \gamma_u$ is within a prescribed tolerance. In this manner, we generate the load-deflection curve in the post buckling regime.

Figure Titles

Fig. 1 The fiber reinforced composite represented by a layered medium.

Fig. 2 The shear-mode buckling configuration.

Fig. 3 Non-linear shear response of PEEK at 21°C. In-situ response is reduced from composite AS4/PEEK data by Kyriakides and Liechti (1993) and compared with the behavior of neat resin.

Fig. 4 The selected discretization of the random distribution expressed in equation (10) into four distinct values of ϕ_f, with average value $\bar{\phi}_f = 0.6$.

Fig. 5 Applied stress vs. non-dimensional maximal lateral deflection v(0)/h. The pre-buckling stage 0A is followed by the post-buckling stage AB.

Fig. 6 Plots of the non-dimensional deflection V vs. the non-dimensional distance X at various levels of applied stress.

Fig. 7 Plots of the non-dimensional slope Y vs. the non-dimensional distance X at various levels of applied stress.

Fig. 8 The distribution of matrix shear stress vs. the non-dimensional distance X within the four distinct cells (——— $\phi_f = 0.175$; ▬▬▬ $\phi_f = 0.45$; o o o o o o $\phi_f = 0.8$; ♦ ♦ ♦ ♦ ♦ ♦ $\phi_f = 0.975$) at various levels of applied stress. 8(a) σ = 654 MPa (pre-buckling), 8(b) σ = 1220 MPa (buckling), 8(c) σ = 730 MPa (post-buckling), and 8(d) σ = 722 MPa (post-buckling. Point B in Figure 5).

Fig. 9 The distribution of fiber shear strain vs. the non-dimensional distance X in the four distinct cells (symbols and stress levels same as in Figure 8).

Fig. 10 Lateral stresses $q_i(x)$ at $\sigma = \sigma_{CR}$ = 1220 MPa vs. the non-dimensional distance X in the four distinct cells. (a) Shear deformable fibers, (b) Fibers deforming as Bernoulli-Euler beams. (o $\phi_f = 0.25$; • $\phi_f = 0.45$; · · · $\phi_f = 0.75$; —— $\phi_f = 0.975$).

Fig. 11 Non-dimensional fiber curvatures (dY/dX) vs. non-dimensional distance X at four levels of applied stress in the pre-buckling range (· · · · · · σ = 654 MPa; ———— σ = 941 MPa; ●●●●● σ = 1021 MPa; ———— σ = 1220 MPa (buckling)). (a) Uniformly spaced fibers with $\phi_f = 0.6$. (b) Randomly spaced fibers (according to Figure 4) with $\bar{\phi}_f = 0.6$.

Fig. 12 Variation of compressive strength (= buckling load) with fiber volume fraction ϕ_f (= $\bar{\phi}_f$ in randomly spaced case). Comparison between uniformly and randomly spaced cases.

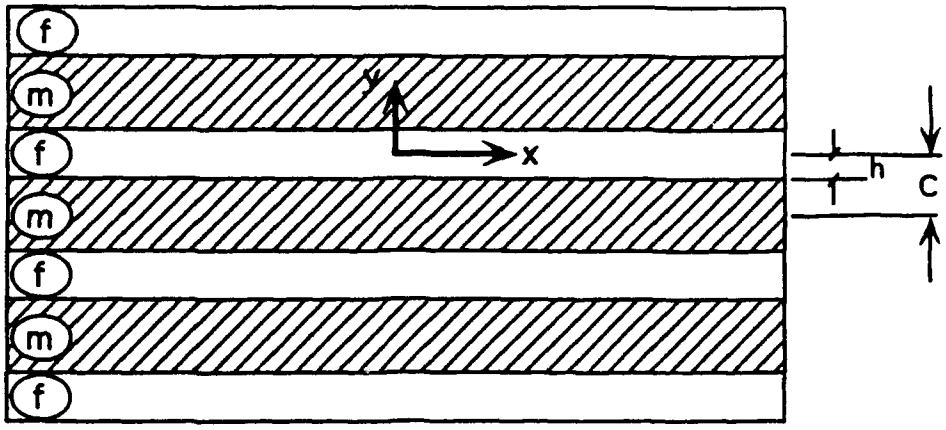

Fig. 1 The fiber reinforced composite represented by a layered medium.

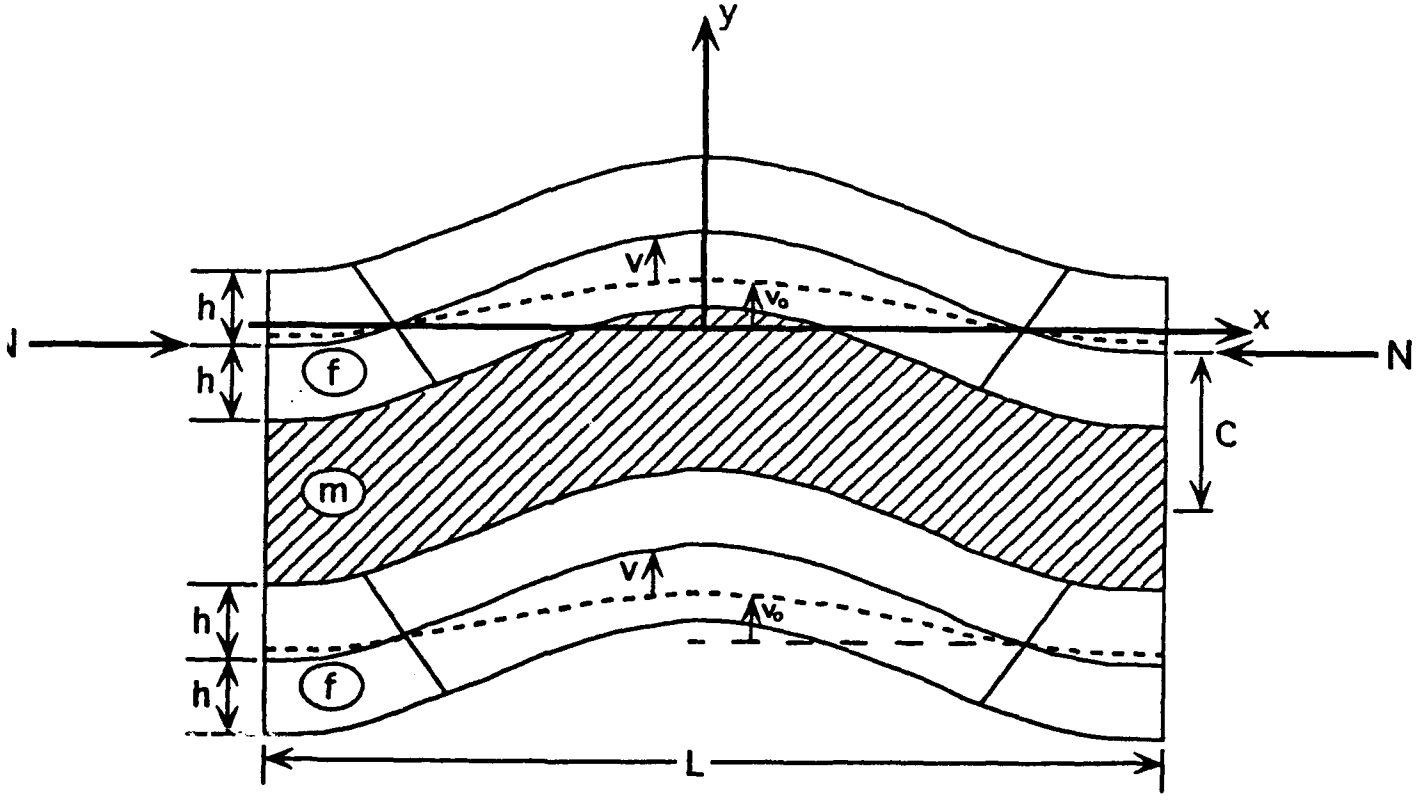

Fig. 2 The shear-mode buckling configuration.

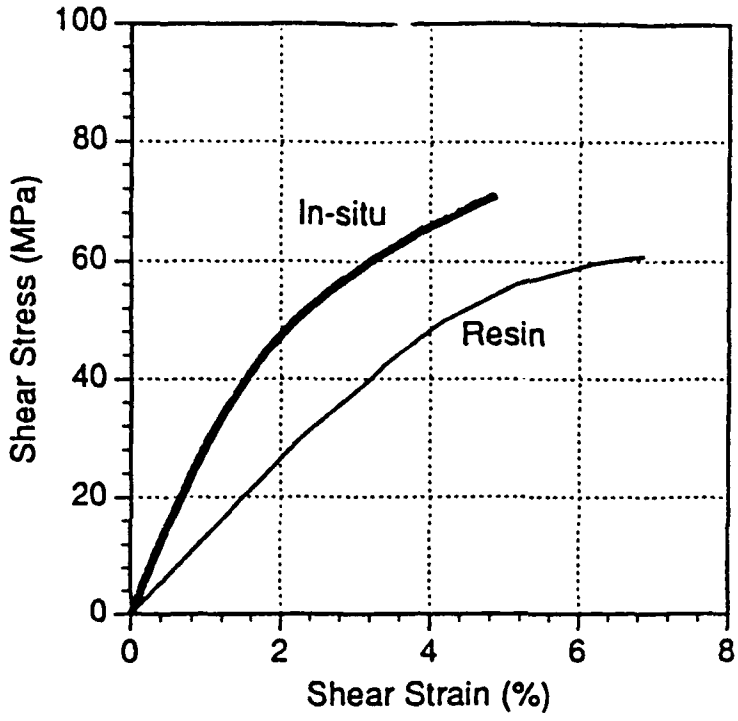

Fig. 3 Non-linear shear response of PEEK at 21°C. In-situ response is reduced from composite AS4/PEEK data by Kyriakides and Liechti (1993) and compared with the behavior of neat resin.

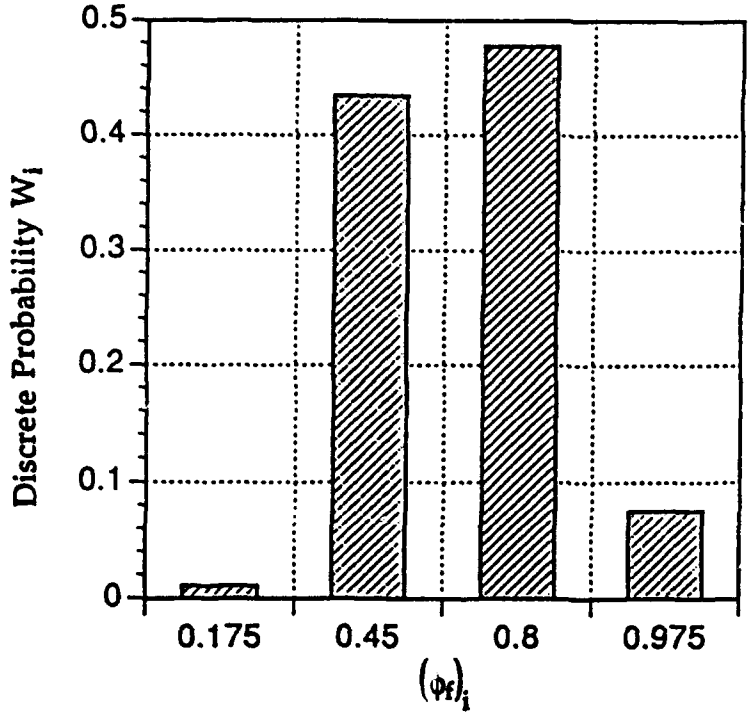

Fig. 4 The selected discretization of the random distribution expressed in equation (10) into four distinct values of ϕ_f, with average value $\bar{\phi}_f = 0.6$.

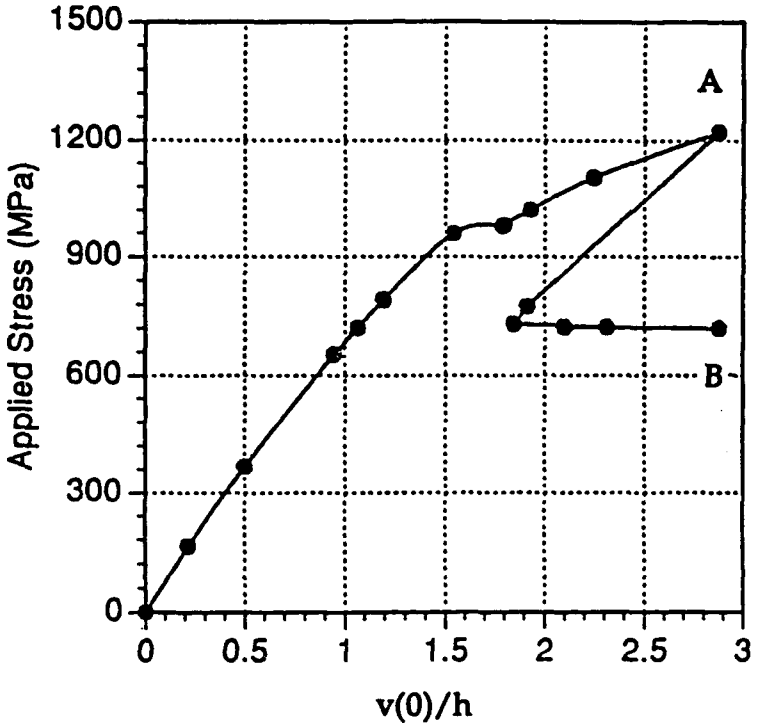

Fig. 5 Applied stress vs. non-dimensional maximal lateral deflection v(0)/h. The pre-buckling stage 0A is followed by the post-buckling stage AB.

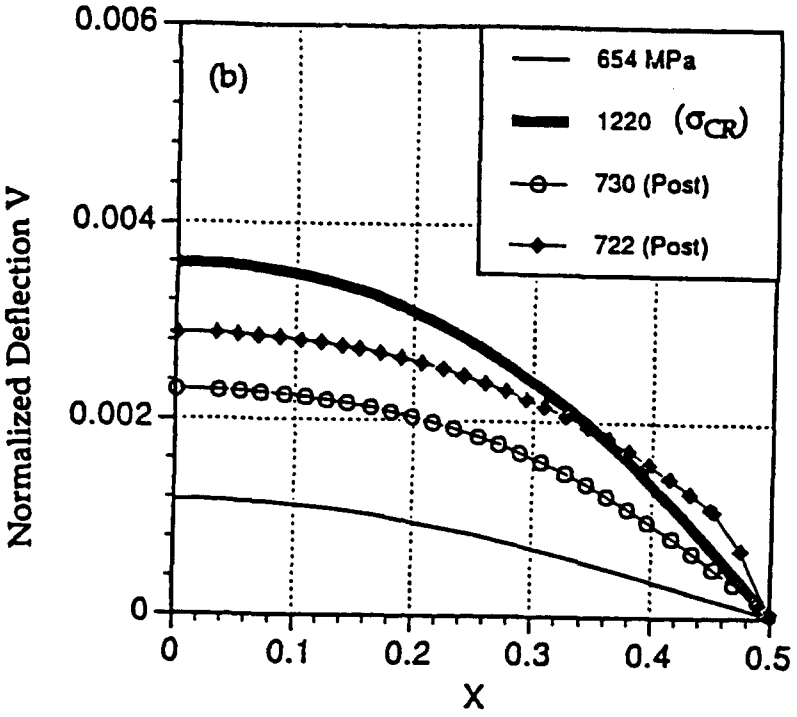

Fig. 6 Plots of the non-dimensional deflection V vs. the non-dimensional distance X at various levels of applied stress.

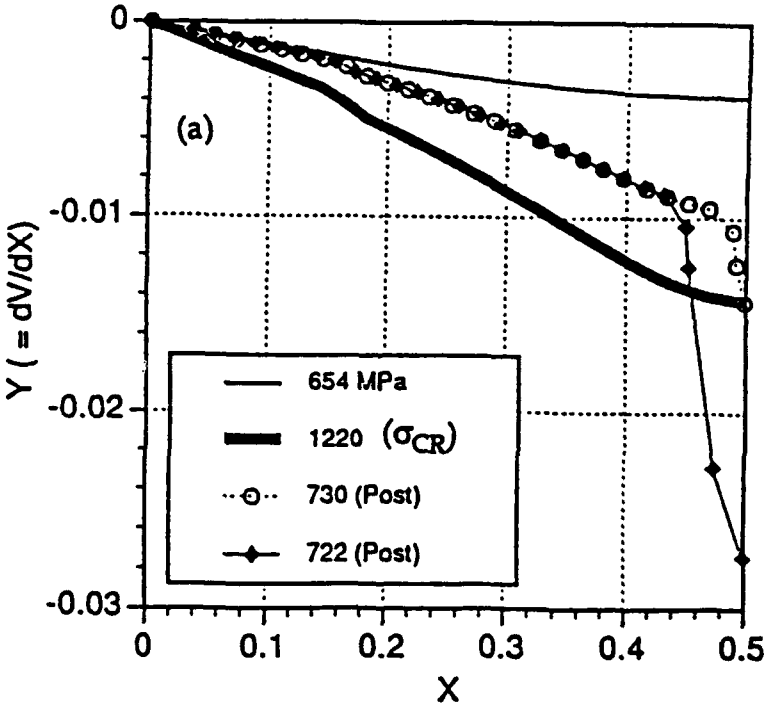

Fig. 7 Plots of the non-dimensional slope Y vs. the non-dimensional distance X at various levels of applied stress.

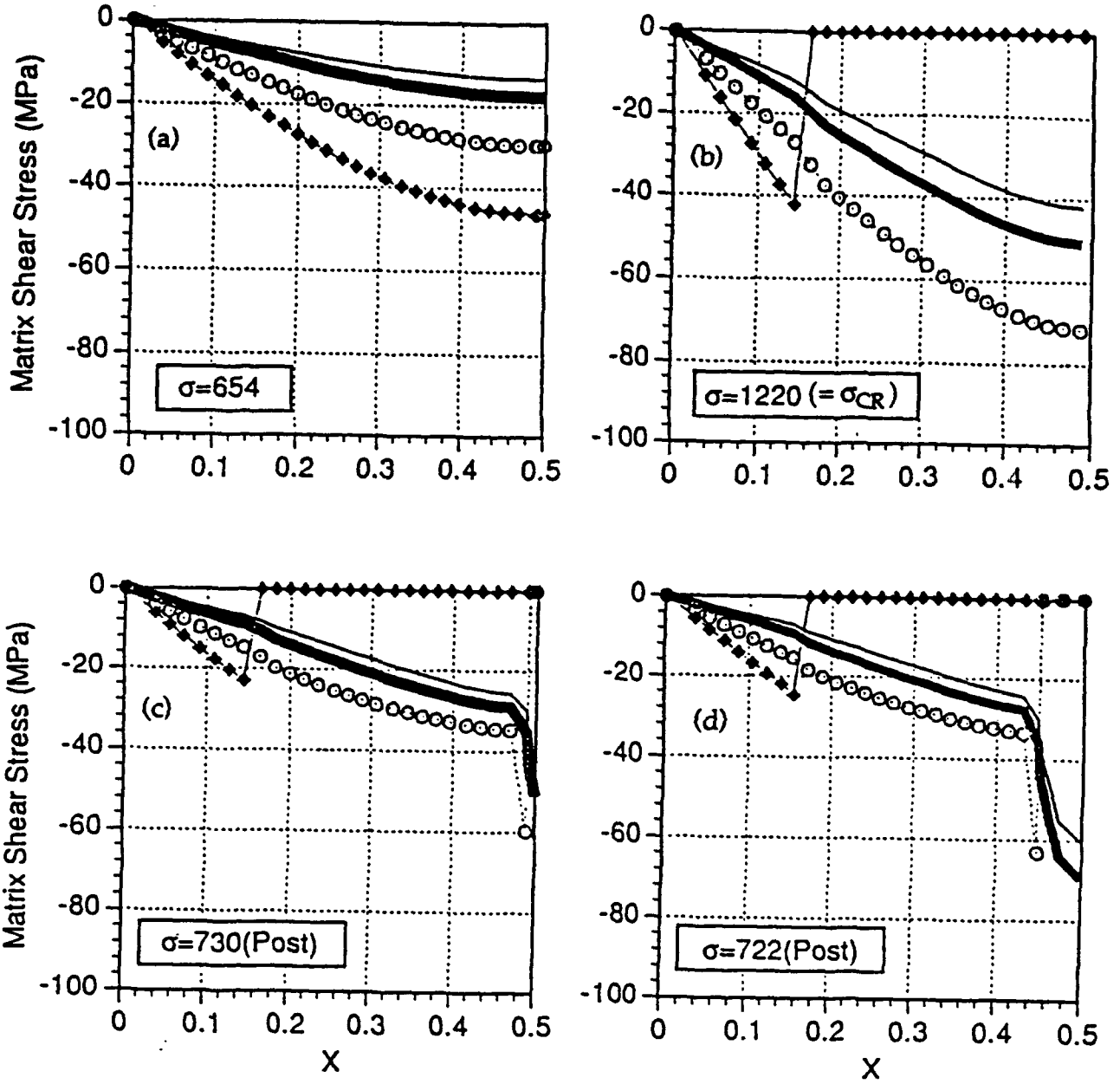

Fig. 8 The distribution of matrix shear stress vs. the non-dimensional distance X within the four distinct cells (——— $\phi_f = 0.175$; ▬▬▬ $\phi_f = 0.45$; o o o o o $\phi_f = 0.8$; ♦ ♦ ♦ ♦ ♦ $\phi_f = 0.975$) at various levels of applied stress. 8(a) σ = 654 MPa (pre-buckling), 8(b) σ = 1220 MPa (buckling), 8(c) σ = 730 MPa (post-buckling), and 8(d) σ = 722 MPa (post-buckling. Point B in Figure 5).

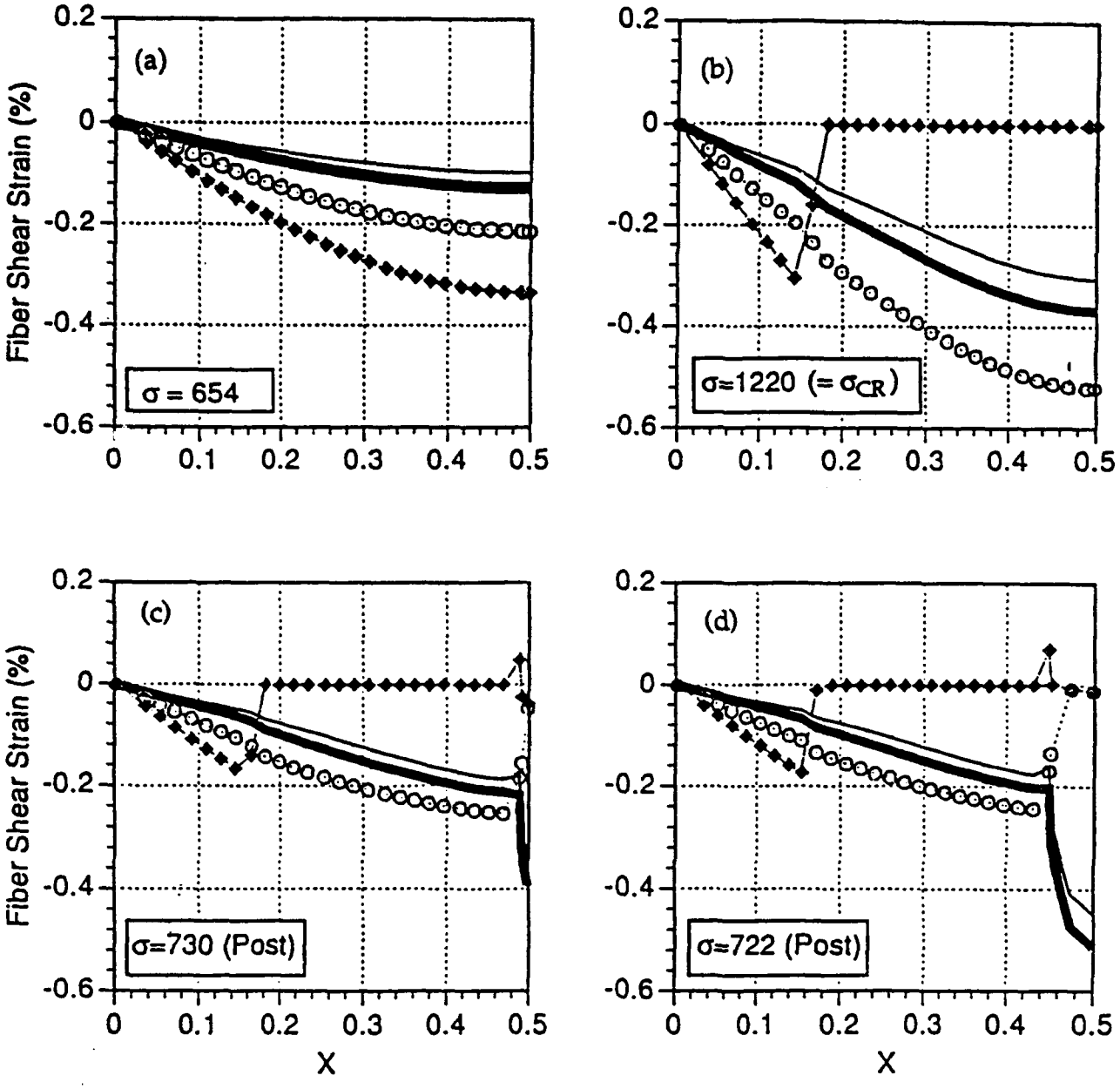

Fig. 9 The distribution of fiber shear strain vs. the non-dimensional distance X in the four distinct cells (symbols and stress levels same as in Figure 8).

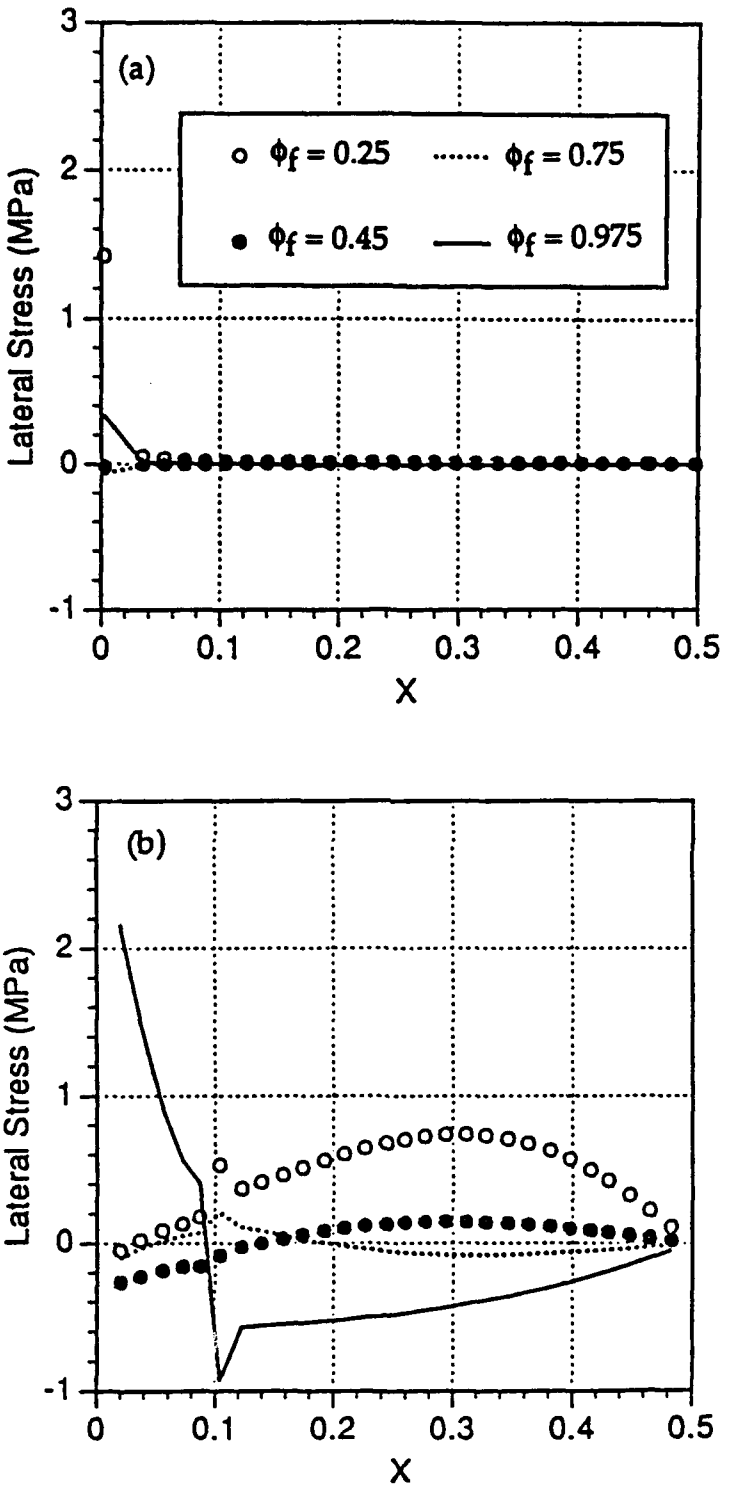

Fig. 10 Lateral stresses $q_i(x)$ at $\sigma = \sigma_{CR} = 1220$ MPa vs. the non-dimensional distance X in the four distinct cells. (a) Shear deformable fibers, (b) Fibers deforming as Bernoulli-Euler beams.
(o $\phi_f = 0.25$; • $\phi_f = 0.45$; $\cdots$ $\phi_f = 0.75$; —— $\phi_f = 0.975$).

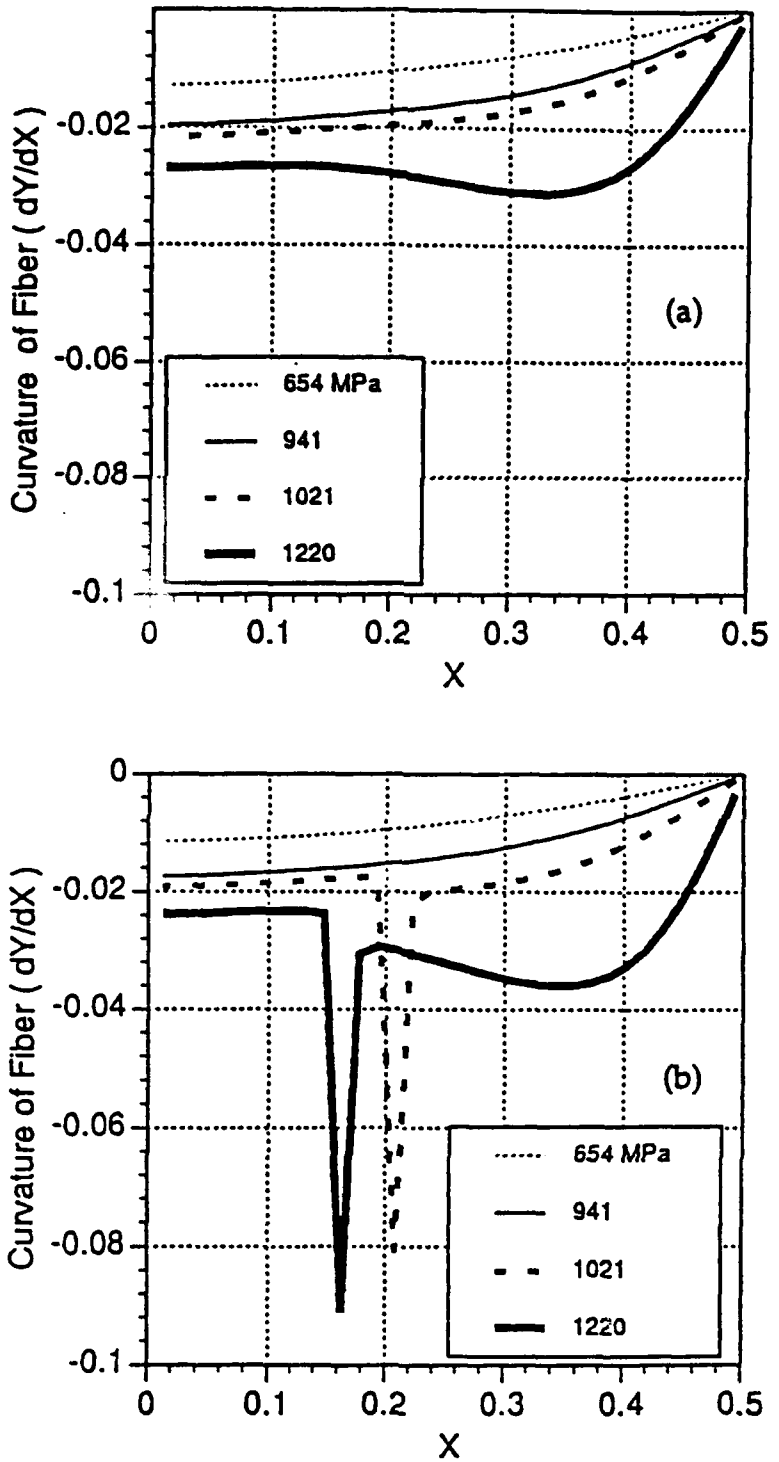

Fig. 11 *Non-dimensional fiber curvatures (dY/dX) vs. non-dimensional distance X at four levels of applied stress in the pre-buckling range* (····· σ = 654 MPa; ——— σ = 941 MPa; ●●●●● σ = 1021 MPa; ——— σ = 1220 MPa (buckling)). (a) Uniformly spaced fibers with $\phi_f = 0.6$. (b) Randomly spaced fibers (according to Figure 4) with $\bar{\phi}_f = 0.6$.

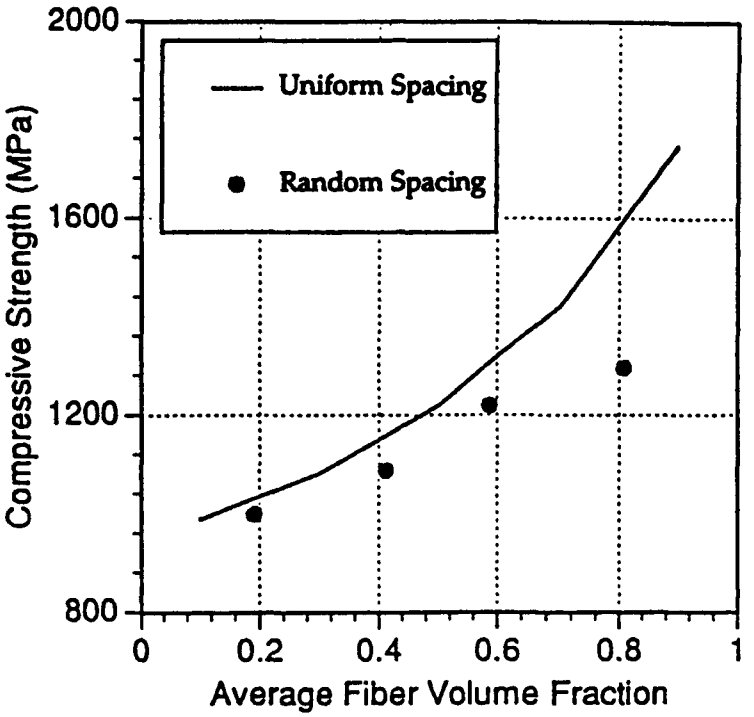

Fig. 12 Variation of compressive strength (= buckling load) with fiber volume fraction ϕ_f (= $\bar{\phi}_f$ in randomly spaced case). Comparison between uniformly and randomly spaced cases.